Journal of King Saud University – Science 35 (2023) 102583

HOSTED BY

Contents lists available at ScienceDirect

Journal of King Saud University – Science

journal homepage: www.sciencedirect.com

Original article

A selective toxicity of Pt-coated Au nanoparticles in cancerous MCF-7 cells over non-cancerous HUVE cells

Mohd Javed Akhtar [a,*], Maqusood Ahamed [a], Hisham Alhadlaq [b]

[a] King Abdullah Institute for Nanotechnology, King Saud University, Riyadh 11451, Saudi Arabia
[b] Department of Physics and Astronomy, College of Sciences, King Saud University, Riyadh 11451, Saudi Arabia

ARTICLE INFO

Article history:
Received 14 November 2022
Revised 18 December 2022
Accepted 29 January 2023
Available online 1 February 2023

Keywords:
Cancer cells
Normal cells
Nitric oxide
Apoptosis
Necrosis
Anticancer

ABSTRACT

Objectives: Nitric oxide (NO) and NO-generated reactive nitrogen species (RNS) in conjunction with reactive oxygen species (ROS) have received attention for their potential in oxidative stress-based cancer therapy. Here, we report commercially obtained Pt-coated Au nanoparticles (Pt-Au NPs; 27 ± 20 nm) higher uptake and cytotoxicity in human breast cancer MCF-7 cells as compared to a non-cancerous human cell (HUVE).

Methods: Cytotoxicity was evaluated by MTT bioassay followed by measurement of ROS (by DCFH-DA probe) and NO (by DAR-2 probe) in live cells. Membrane integrity was evaluated by measuring lipid peroxidation by live cell dye BODIPY fluorescence, TBARS absorbance, and LDH release. Ubiquitous antioxidant GSH was also measured followed by changes in MMP status by live cell dye JC-1. Mode of cell death was determined by triple staining (Hoechst/annexin V/PI triple staining), and caspase 9 and 3 activities in cancerous MCF-7 and non-cancerous HUVE cell lines.

Results: MCF-7 cells exhibited a 63 ± 5 % higher tendency of Pt-Au NPs uptake in comparison to HUVE cells. Accordingly, IC50 of Pt-Au NPs came out to be 0.48 ± 0.09 μM in MCF-7 cells and 0.93 ± 0.11 μM in non-cancerous HUVE cells. Therefore, the cytotoxic potential of NPs in MCF-7 cells was almost 1.9-fold higher than in HUVE cells indicating cancer cells are significantly more susceptible to death than HUVE cells with a normal tissue origin. NPs caused a significant induction in oxidative stress and loss in MMP in the two cells.

Conclusion: We realize two major facts from this study that goes in the favor of anticancer potential of Pt-Au NPs. The first reason is the high internalization of NPs in MCF-7 cells as compared to that in HUVE cells. The second reason is that HUVE cells were found not as expressive for NO as were MCF-7 cells.

1. Introduction

Nanoparticles (NPs; defined as particles having at least one dimension below 100 nm) have been manufactured by nanotechnology technique. These NPs behave differently in biological models. Interestingly, some of these NPs are toxic to all cells such as quantum dots while some are discriminatory. Discriminatory NPs exert toxicity to cancer cells at the concentration at which there occurs no significant toxicity in primary or non-cancerous cell lines (Xu et al., 2019). These NPs are considered to have great potential in cancer therapy. Anticancer NPs leads to a preferential death in tumorigenic cells as compared to the death induced in normal cells. Oxidative stress arises due to the production of high concentrations of harmful oxidants that exceed the cellular antioxidant capacity. Strategies of increasing further reactive oxygen species (ROS) in cells that are already burdened with numerous kinds of oxidants could serve as an anticancer therapy in cells with high metabolic activity like proliferating cancer cells (Galadari et al., 2017).

In this study, we, therefore, carried out a comparative study in cancerous MCF-7 and non-cancerous HUVE cells to observe any potential mechanism of toxicity based on differential production of ROS and accompanied mechanism therein as carried out by several investigators (Rawal et al., 2019). Moreover, a review of available data suggests that NPs exhibit versatile responses upon

* Corresponding author at: King Abdullah Institute for Nanotechnology (KAIN) King Saud University, P.O. Box 2454, Riyadh 11451, Saudi Arabia.
E-mail addresses: mohd.j.akhtar@gmail.com, mjakhtar@ksu.edu.sa (M.J. Akhtar).

Peer review under responsibility of King Saud University.

Production and hosting by Elsevier

https://doi.org/10.1016/j.jksus.2023.102583
1018-3647/

interaction with cells whose function requires possession of a differentiated set of biological machinery (Akhtar et al., 2018). This study was advanced by selecting a battery of relevant parameters as briefly summarized here. Cytotoxicity was evaluated by MTT bioassay followed by measurement of ROS (by DCFH-DA probe) and NO (by DAR-2 probe) in live cells. Membrane integrity was evaluated by measuring lipid peroxidation (LPO) by live cell dye BODIPY fluorescence, thiobarbituric acid reactive substances (TBARS) absorbance, and lactate dehydrogenase (LDH) release. Ubiquitous antioxidant reduced glutathione (GSH) was also measured followed by changes in mitochondrial membrane potential (MMP) by live cell dye JC-1. Mode of cell death was determined by triple staining (Hoechst/annexin V/PI triple staining), and caspase 9 and 3 activities in cancerous MCF-7 and non-cancerous HUVE cell lines.

2. Materials and methods

2.1. Chemicals and reagents

Fetal bovine serum, calcein-AM, and penicillin–streptomycin were purchased from Invitrogen Co. (Carlsbad, CA, USA). DMEM F-12, MTT [3-(4,5-dimethyl thiazol-2-yl)-2,5-diphenyl tetrazolium bromide], NADH, pyruvic acid, perchloric acid, DCFH-DA, DAR-2 (4,5-Diamino-N,N,N′,N′-tetraethylrhodamine), JC-1, glutathione (GSH), o-phthalaldehyde (OPT), hank's balanced salt solution (HBSS), caspase substrates, Bradford reagent and Pt-coated Au NP (27 ± 20 nm) were purchased from a commercial source (Sigma–Aldrich, MO, USA). An apoptosis/necrosis triple staining kit was obtained from BD biosciences (USA). Ultrapure water was prepared in a Milli-Q system (Millipore, Bedford, MA, USA). All other chemicals used were of reagent grade.

2.2. Internalization of Pt-Au NPs in cells

Cell internalization of Pt-NPs was detected according to the method described for the internalization of similar NPs of platinum-tethered Au (Brown et al., 2010). The two cells were exposed to NPs for 4 h to avoid induction of any toxicity. Now cells were carefully washed in cold PBS to remove excess NP. Carefully washed cells were lysed in 0.5 mL of 1 % triton-100X aqueous solution and digested in a final concentration of 50 % HNO_3. Samples were analyzed by ICP-MS for Au metal content, the main constituent of NP, as a marker of the degree of internalization of NPs.

2.3. Cell culture and treatment with Pt-Au NPs

The two cells (MCF-7 and HUVE; ATCC, US) were cultured in DMEM-F12 that was complemented with 10 % FBS, 100 U/mL penicillin, and 100 μg/mL streptomycin. HUVE cells additionally received endothelial growth components (CADMEC, Cell Applications, Inc., San Diego, CA, USA). Cells were incubated at 37 °C in a 5 % CO_2 incubator with proper humidity. The cells were passaged every 3–4 days. Cells were exposed to Pt-Au NPs (27 ± 20 nm; Sigma–Aldrich, MO, USA) for a period of 24 h.

2.4. Determination of cell viability by MTT

Cells (2×10^4/96 well) were exposed to NPs for 24 h and cell viability was determined as illustrated by Mosmann (1983). After the exposure period was over, cells were added and incubated with MTT salt for 2 h in which live cells convert yellow MTT to blue formazan crystals. Formazan crystal, thus, formed by viable cells was solubilized in 20 % SDS prepared in 50 % dimethylformamide. Solubilized formazan is quantified at 570 nm in a plate reader (Synergy HT, Bio-Tek, Winooski, VT, USA). Cell viability is directly proportional to the intensity at 570 nm and is expressed as a percent of control. IC50s calculations for the NPs and H_2O_2 were made from the online IC50 calculator (https://www.aatbio.com/tools/ic50-calculator) provided by AAT Bioquest, Inc. (CA 94085, USA). Cells were also imaged by phase contrast microscopy.

2.5. Detection of intracellular ROS

The potential induction of ROS was detected by utilizing cell-permeable dye 2′, 7′-dichlorofluorescin diacetate (DCFH-DA) as described (Wang and Joseph, 1999). Inside cells, this dye is cleaved to DCFH and acetate and becomes cell impermeable. DCFH becomes fluorescent DCF after oxidation by cellular ROS. The dye was incubated for 60 min at the final concentration of 50 μM. Now emitting fluorescence was quantified at 528 nm in a plate reader (Synergy HT, Bio-Tek, Winooski, Vermont, USA). ROS is directly proportional to DCF fluorescence and is expressed as a percent of control.

2.6. Measurement of intracellular GSH

Antioxidant GSH was detected by its reaction with thiol-reactive o-phthalaldehyde (OPT) that produces fluorescent GSH-adduct as described by Hissin and Hilf (1976). In brief, different cell groups were collected from a 6-well plate, washed, and lysed in 0.1 % deoxycholic acid plus 0.1 % sucrose and centrifuged at 10,000 × g for 10 min at 4 °C. Lysate was centrifuged to get a cell-debris free supernatant. In the supernatant, GSH was determined by treating with OPT in a buffer of (0.1 M phosphate–5 mM EDTA, pH 8.3. GSH adduct was quantified at an emission wavelength of 460 nm (Synergy HT, Bio-Tek, Winooski, Vermont, USA) and presented as GSH (nmol/mg protein). A GSH standard was similarly run.

2.7. Intracellular NO detection

Intracellular NO was quantified by a rhodamine-based live cell-permeable fluorescent probe DAR-2 that reacts specifically with intracellular NO generating an intense fluorescence in the infrared region (Kojima et al., 2001; Li and Wan, 2015; Von Bohlen and Halbach 2003). Cells in a 12-well plate were labeled with DAR-2 at a final concentration of 15 μM for 2 h. Cells were also co-labeled with live cell fluorescent probe calcein-AM at 1 μM corroborating cell viability with NO production. Live cells were imaged under a microscope with a suitable filter cube (Leica DMi8, Wetzlar, Germany).

2.8. Analysis of membrane integrity

The integrity of cell membrane can be assessed in many ways that are not only complemented by each other but provides detailed mechanism too. Membrane integrity was assessed by quantifying the release of lactate dehydrogenase enzymes in cell culture media as described by Welder (1992). Cell membrane damage results mainly from the peroxidation reactions initiated by the free radical category of ROS in poly-unsaturated fatty acids of the lipid bilayer. Therefore, LPO was recorded by quantifying TBARS as described by Ohkawa et al (1979). Membrane damage was also analyzed by more modern methods. One method is the application of lipophilic dye BODIPY581/591 probe that produces green fluorescence in a proportion of ROS residing mainly in membranes (Akhtar et al., 2020; Sayes et al., 2005; Raudsepp et al., 2014). Cells were incubated with 2 μM of dye for 60 min and imaged under a fluorescent microscope (Leica DMi8 manual, Germany).

Table 1
Summary of physicochemical properties of Pt-Au NPs.

Parameters	Physico-chemical properties
Colour	Dark bluish in liquid
TEM (size)	26 ± 21 nm
TEM (shape)	Mainly cubes and some partially spherical
XRD	Crystalline (average crystallite size; 27 ± 19 nm)
Pt to Au concentration ratio	Almost 1:1 (as per data provided from supplier)
DLS in complete culture media	
Hydrodynamic size	149 ± 58 nm
Zeta potential	−38 ± 5 mV
DLS in water	
Hydrodynamic size	201 ± 76 nm
Zeta potential	−26 ± 5 mV

2.9. The detection of the membrane potential of mitochondria

Potential changes in the mitochondrial membrane that could occur due to the exposure of NPs in the two cells were determined by the application of ratio-metric dye JC-1 (Smiley et al., 1991). In brief, cells were removed with NPs by gentle washing in HBSS buffer. Now cells were incubated with 5 μM of JC-1 for 20 min and imaged under a fluorescence microscope (Leica DMi8 manual, Germany).

2.10. Analysis of apoptosis/necrosis pathways

The mode of cell death due to the exposure of NPs in the two cells was resolved by triple staining (Hoechst/Annexin-FITC/PI) technique as described by Atale et al., (2014). In this method, the mode of cell death is deciphered by the concurrent presence/absence of particular dyes (Crowley et al., 2016a; Sawai and Domae, 2011; Darzynkiewicz et al., 1992; Fink and Cookson,

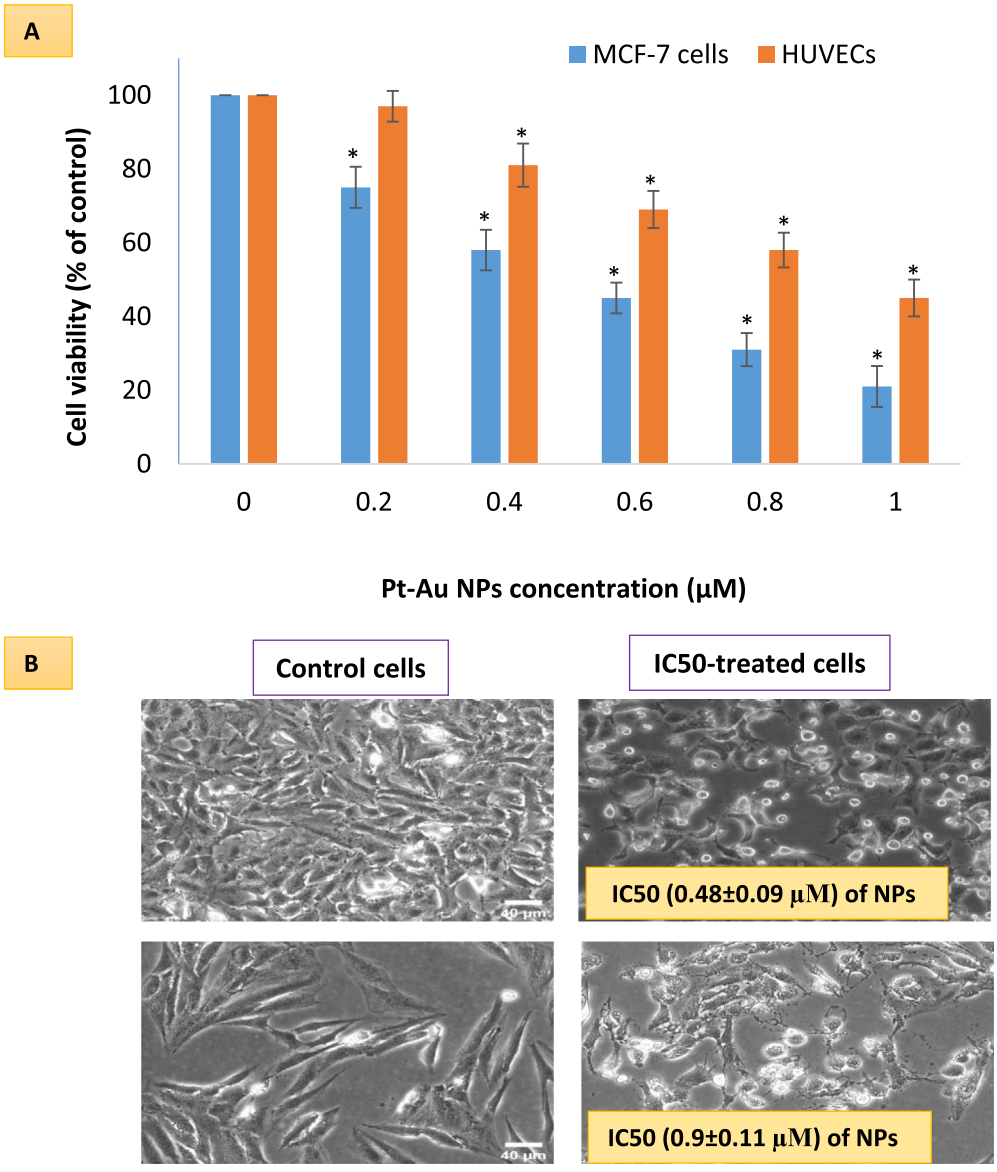

Fig. 1. Comparative cell viabilities in two cell lines- one with cancer origin (MCF-7 cell), and the other with non-cancerous origin (HUVE Cells) as evaluated by MTT assay (A). The highest toxicity occurred in MCF-7 cells while lesser toxicity in HUVE cells. IC50 was calculated using an online calculator (https://www.aatbio.com/tools/ic50-calculator) provided by AAT Bioquest, Inc. (CA 94085, USA). IC50 of Pt-Au NPs in MCF-7 was 0.48 ± 0.09 μM and IC50 in HUVE cells was 0.93 ± 0.11. Data represented are mean ± SD of three identical experiments (n = 3) made in triplicates. *statistically significant difference as compared to the controls ($p < 0.05$).

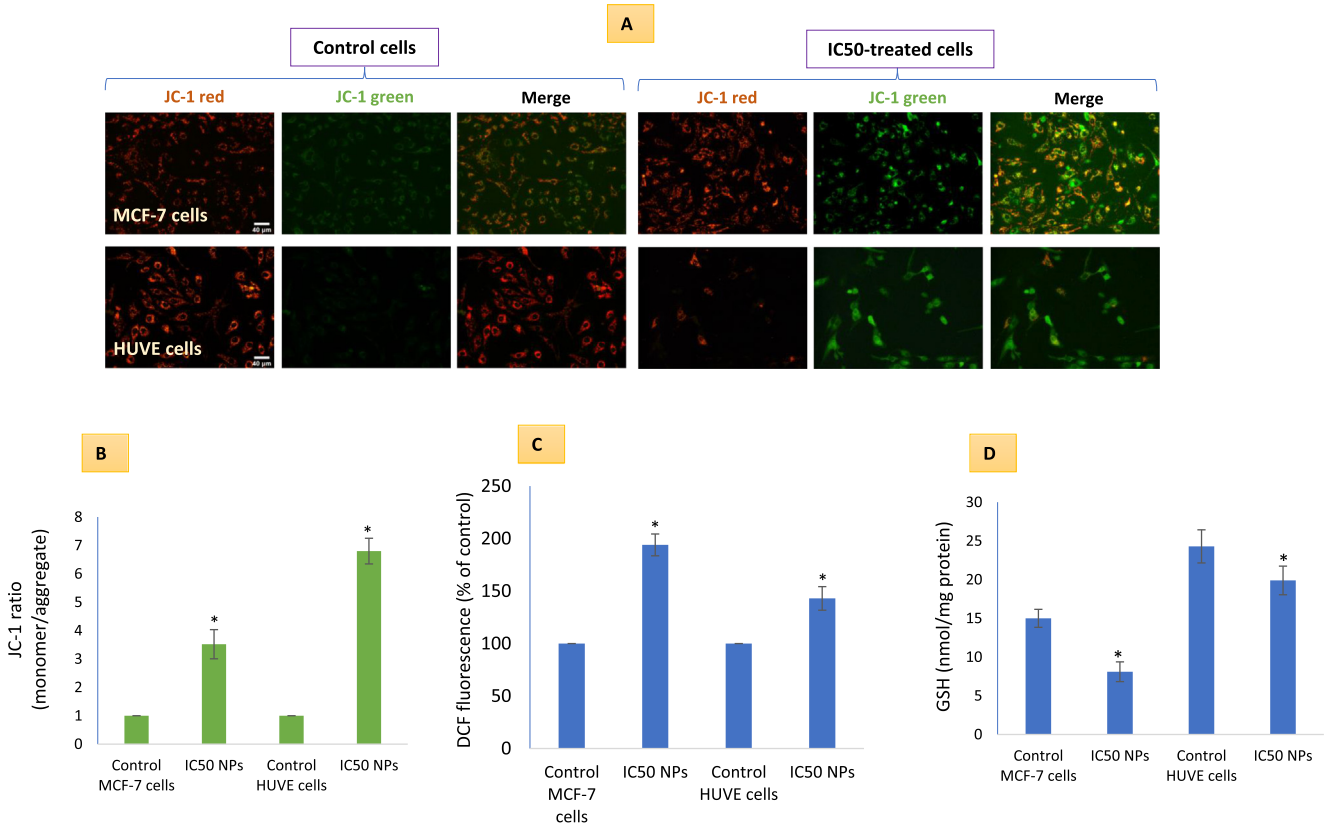

Fig. 2. MMP loss due Pt-Au NPs exposure in cells was evaluated by applying a radiometric dye JC-1 in live cells (A). A higher fluorescence in green is positively related to a high loss in MMP as given in (B). ROS-induction (C) and GSH-depletion (D) due to NPs in the two cells reflect the mechanism of high sensitivity in MCF-7 cells. It is worth mentioning that IC50 of Pt-Au NPs in MCF-7 was 0.48 ± 0.09 μM and IC50 in HUVE cells was 0.93 ± 0.11 under similar conditions of treatment making MCF-7 cells almost 1.9-fold more sensitive to NPs as compared to HUVE cells. The scale bar, marked only in starting images as a general convention, represents 40 μm captured by a 20 × objective. Data represented are mean ± SD of three identical experiments (n = 3) made in triplicates. *statistically significant difference as compared to the controls ($p < 0.05$).

2005). After treatment time was completed, each cell group was gently washed and then incubated with Annexin-FITC for 20 min. After removing excess Annexin dye, cells were loaded with Hoechst and PI each at 1 μg/ml. Now cells were imaged for each dye under suitable filter cubes of the microscope. This is an inexpensive and dependable method that was successfully applied in our previous publication (Akhtar et al., 2020). Activities of caspase 9 and 3 are upregulated in caspase-dependent apoptosis whereas necrosis is caspase-independent. Treated and control cells were analyzed for the activities of caspase 9 and caspase 3 using their respective fluorescent substrates (Ac-LEHD-AFC for caspase 9 and Ac-DEVDAFC for caspase-3). Fluorescent intensity was recorded for 20 min taking a reading at every 5 min interval in a plate reader. (Synergy HT, Bio-Tek, Winooski, Vermont, USA). Activities of caspases are given in % age of control.

2.11. Protein estimation

The total protein content was measured by a convenient BCA Protein Assay Kit from Sigma-Aldrich as per instructions.

2.12. Statistics

Statistical analysis was performed by analyzing ANOVA (one-way analysis of variance) and Dunnett's multiple comparison tests. For imaging analysis, a burst of images was taken and corrected total cellular fluorescence (CTCF) was calculated using open-source free ImageJ software provided by NIH, Bethesda, MD, US. CTCF was calculated from individual cell fluorescence that got subtracted acellular background mean fluorescence. Imaging was performed under constant exposure time, gain, and light intensity.

3. Results

3.1. Higher uptake of NPs in MCF-7 cancer cells than in non-cancerous HUVE cells

In this study, MCF-7 cells exhibited a 63 ± 5 % higher tendency of NPs uptake in comparison to HUVE cells in an indirect estimation of comparative NP internalization experiment based on the analysis of the main constituent of NPs (i.e. Au) by ICP-MS. According to its supplier (Sigma-Aldrich, MO, US) description, the concentration of gold was 45.0–55.0 ppm in a product (Pt-Au NP) concentration of 90.0–110.0 ppm. Physico-chemical properties of Pt-Au NPs are summarized in Table 1.

3.2. MCF-7 and HUVE cells exhibited concentration-dependent cytotoxicity with different sensitivities

The IC50 of NPs in MCF-7 cells came out to be 0.48 ± 0.09 μM for a 24 h treatment period. HUVE cells with normal origin exhibited a higher resistance towards Pt-coated Au NPs; the IC50 of NPs in HUVE cells came out to be 0.93 ± 0.11 μM for a 24 h treatment period (see Fig. 1A). When the IC50s of two cell lines were compared, IC50 in HUVE cells was found to be 1.9 times higher than that of IC50 in MCF-7 cells. From the cytotoxicity data, it is clear that the most sensitive cells to NPs were MCF-7 cells whereas the least sensitive cells were HUVE cells. This cell viability data indicate that NPs do have

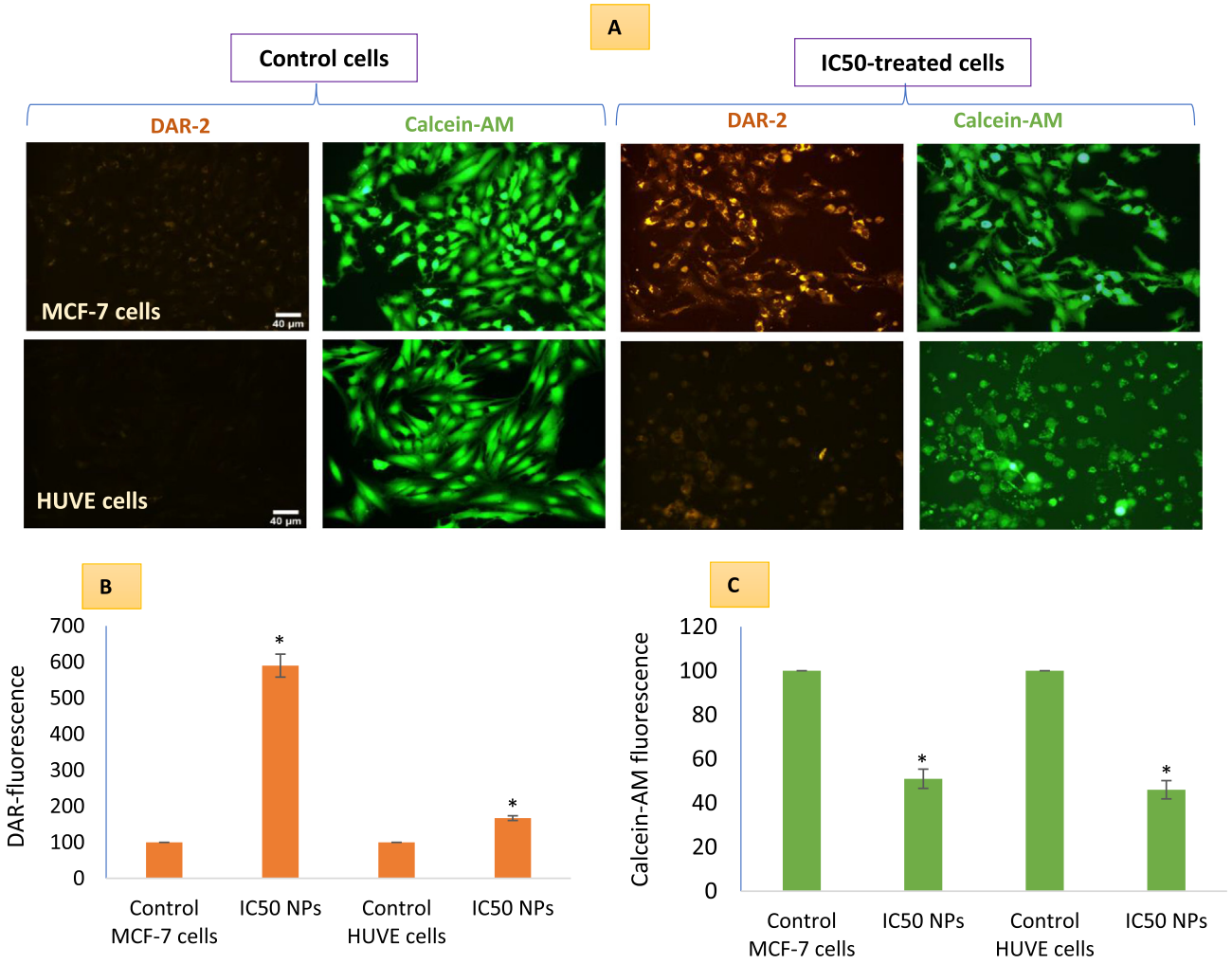

Fig. 3. NO-generation due to Pt-coated Au NPs treatment in MCF-7 and HUVE cells was detected by applying a NO-specific DAR-1 fluorescent probe that turns fluorescent (far-red images) after reacting with NO. For each DAR-1 image, a superimposable image under live cell dye calcein-AM (green images) was captured corroborating NO production with the degree of cell viability. Quantitative data of DAR-1 and calcein-AM fluorescence is presented in B and C respectively. It is worth mentioning that IC50 of Pt-Au NPs in MCF-7 was 0.48 ± 0.09 µM and IC50 in HUVE cells was 0.93 ± 0.11 under similar conditions of treatment making MCF-7 cells almost 1.9-fold more sensitive to NPs as compared to HUVE cells. The scale bar, marked only in control images as a general convention, represents 40 µm captured by a 20 × objective. Data represented are mean ± SD of three identical experiments (n = 3) made in triplicates. *statistically significant difference as compared to the controls ($p < 0.05$).

anticancer potential as for as the *in vitro* results are concerned. Phase contrast image is provided as pair of control and treated with IC50 of NPs for each cell line in Fig. 1B. To understand NP-mediated ROS-based approaches in anticancer therapy, we carried out the following relevant parameters in the two human cells- MCF-7 and HUVE cells- as a representative model of cancer cells and non-cancerous cells respectively. The two cell lines were exposed to Pt-coated Au NPs for 24 h at their respective IC50s.

3.3. Pt-coated Au NPs significantly induced a loss in mitochondrial membrane potential (MMP), ROS, and GSH depletion in MCF-7 cells and HUVE cells at their respective IC50s

MMP in MCF-7 cells and HUVE cells was determined by ratio metric JC-1 imaging (Fig. 2A) and calculating the ratio of JC-1 monomer/aggregate (Fig. 2B). In both cell lines, MMP loss was higher when compared to respective control cells. MMP loss was found to occur 6.5-fold in MCF-7 cells whereas 6.8-fold in HUVE cells due to IC50s of NPs. Pt-coated Au NPs caused significant induction of ROS as measured by DCF fluorescence (Fig. 2C) in both MCF-7 cells and HUVE cells. Induction of ROS was 1.9-fold in MCF-7 cells while 1.3-fold in HUVE cells due to their respective IC50s exposures. Data suggest that ROS occurred at a higher level in MCF-7 cells in comparison to HUVE cells. These NPs also depleted GSH significantly in the two cells (Fig. 2D). GSH level was reduced to 54 % in MCF-7 cells while it was still 88 % in HUVE cells when exposed at their respective IC50s of NPs. Data again suggest that GSH depletion occurred to be steeper in MCF-7 cells in comparison to HUVE cells. Several studies suggest that the generation of ROS exerts more detrimental effects than the depletion of GSH in cells (Okon and Zou, 2015).

3.4. Pt-coated Au NPs significantly induced NO in MCF-7 cells while it was much lower in HUVE cells

These NPs came out to be a strong inducer of NO in MCF-7 cells whereas NO induction was lesser in HUVE Cells (Fig. 3A). NPs caused almost 6-fold induction of NO (see images for DAR-1 fluorescence in the far-red region in 3A and DAR-1 fluorescence calculations in Fig. 3B for respective cells) in treated MCF-7 cells when compared to control MCF-7 cells. NO induction in HUVE cells was 1.6-fold to that of control HUVE cells. As evident from cell images and DAR-1 fluorescence quantification data (see Fig. 3B), treated HUVE cells displayed much less induction of NO as com-

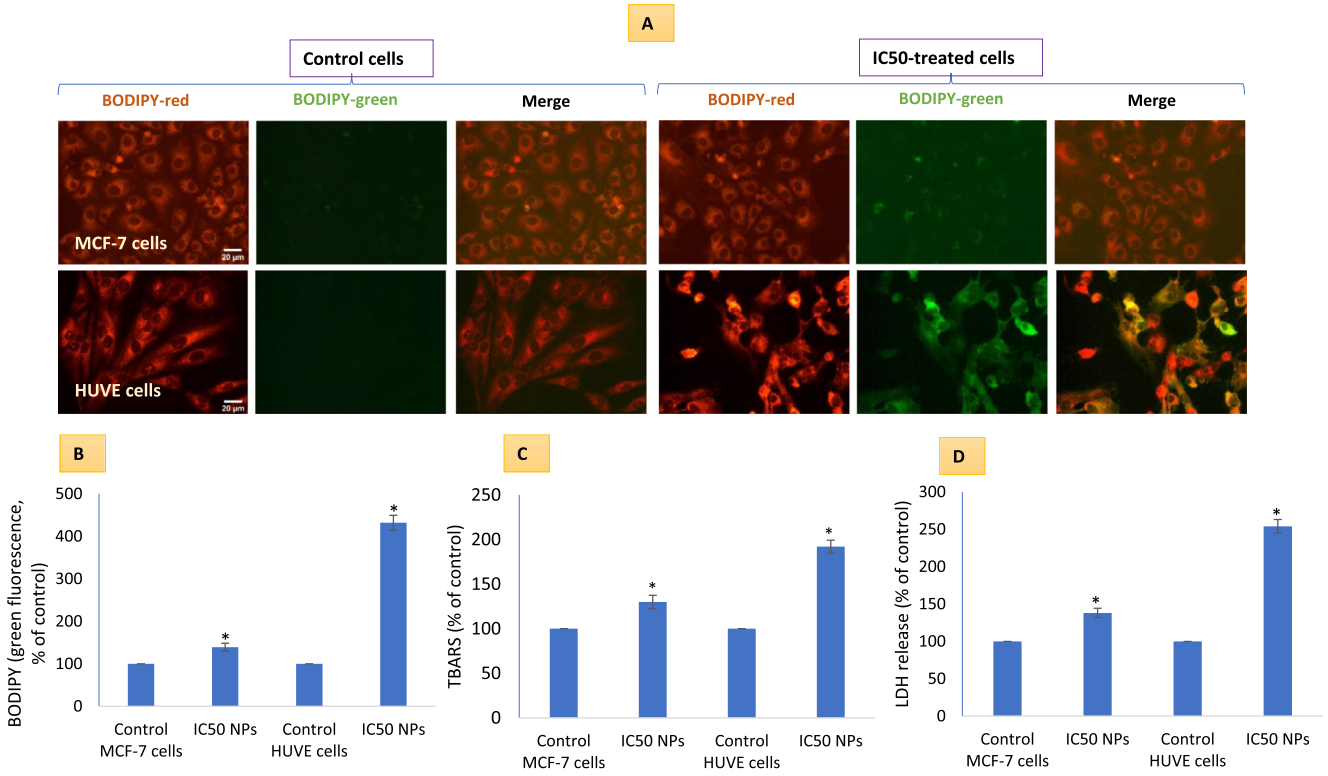

Fig. 4. Cell membrane damaging potential due to Pt-coated Au NPs in MCF-7 and HUVE cells was determined by imaging cells labeled under lipophilic dye BODIPY that give rise to green fluorescence in a proportion of membrane damage (A). Quantitative BODIPY green fluorescence has been given in (B). Membrane damage was also quantified by measuring TBARS (C) and LDH release (D). High membrane damage in less NO-producing HUVE cells can partially be explained by a NO-dependent lack of lipid peroxidation termination in HUVE cells. The scale bar, marked only in control images, represents 20 μm captured by a 40 × objective. Data represented are mean ± SD of three identical experiments (n = 3) made in triplicates. *statistically significant difference as compared to the controls ($p < 0.05$). α denotes significantly high membrane damage in HUVE cells compared to that in MCF-7 cells exposed at the respective IC50s for each cell type.

pared to MCF-7 treated cells. It is worth mentioning that NO upon reaction with ROS can give rise to secondary metabolites collectively known as RNS that could exert a more deleterious effect in MCF-7 cells or, paradoxically, NO can consume superoxide radicals by reacting with them and producing more deleterious peroxynitrite. Moreover, we corroborated NO concentration in each treatment group with the status of cell viability by simultaneously imaging cells labeled with live cells dye calcein-AM (see green fluorescent images in Fig. 3A and calcein-AM quantification in Fig. 3C).

3.5. Membrane damage was steeper in HUVE cells than in NO-expressing MCF-7 cells

Direct observation of membrane damage occurring in cells was observed by labeling cells with membrane residing BODIPY probe that gives brighter green fluorescence in a positive correlation of lipid peroxidation (Fig. 4A). BODIPY green fluorescence quantification (Fig. 4B) suggested significantly higher membrane damage in HUVE cells corroborating with higher ROS. Relatively higher losses in membrane integrity in HUVE cells were again confirmed by quantifying TBARS (Fig. 4C) and LDH releases (Fig. 4D). Recall, NO is a hydrophobic radical molecule that has low reactivity in comparison to other free radicals such as superoxide radicals, and can even terminate lipid peroxidation reactions initiated by strong oxidizing radicals such as hydroxyl radical or nitrogen dioxide radicals (Garrel and Fontecave, 1995).

3.6. Cell death due to NPs was apoptosis-dependent in MCF-7 cells while it was apoptosis-independent in HUVE cells

Treated MCF-7 cells were extensively stained with PI as well as annexin V (Fig. 5A). Recall, cells undergoing apoptosis exhibit intact cell membranes with blebs, and shrinkage in volume, with chromatin tightly packed giving bright and clumped fluorescence whereas cells undergoing necrosis exhibit early cell membrane damage, increased in cell volume with dilated nuclear periphery within which lie circumscribed chromatin that gives diffused fluorescence (Darzynkiewicz et al., 1992; Fink and Cookson, 2005). PI preferentially enters necrotic cells while being excluded from early apoptotic cells that are characterized by annexin V staining without PI (Sawai and Domae, 2011). In Fig. 5A, such cells are only visible in MCF-7 cells (marked with arrows). In the MCF-7 cell panel, many cells are simultaneously stained with both PI and annexin V marking these cells as late-stage apoptotic or secondary necrotic (Crowley et al., 2016b). A closer observation suggested apoptosis-independent cell death in HUVE cells treated with NPs indicated by a smooth fluorescence and dilated nuclear size (Eidet et al., 2014; S. Afifi et al., 2012). Another clue of apoptosis observed in MCF-7 cells is the upregulated levels of caspase 9 (Fig. 5B) and caspase 3 (Fig. 5C) enzymes that are not at the appreciable levels in HUVE cells.

4. Discussion

Pt-Au NPs used in this study were 27 ± 20 nm in size, and were mostly spherical having a little bit longer to breadth ratio. As the name would suggest these NPs of Au were coated with the element

Pt. Such Pt coating to Au NPs is reported to result in an NP's surface that would exhibit enhanced catalysis (Gao et al., 2017). The surface tunable property of gold has been under extensive exploration for improving the uptake of gold NPs as well as modifying it with a variety of other desired anticancer drugs in targeted therapy of cancer (Fan et al., 2020). Data also suggest that Au NP have had a higher propensity of internalization in many cancer cells in comparison to chemical anticancer drugs (Brown et al., 2010). Our findings reveal that cancer MCF-7 cells internalized a greater quantity of NPs in comparison to less sensitive non-cancerous HUVE cells. Data demonstrate a differential sensitivity and mechanism of action in cancer MCF-7 cells being the most sensitive one in comparison to normal cell line HUVE cells being the less susceptible to death induced by NPs. A similar selectivity was observed for Au NPs (Fan et al., 2020) as well as Pt NPs (Bendale et al., 2017; Ullah et al., 2017) in different cancer cells while sparing primary normal cells. Generation of ROS and exhaustion of antioxidant GSH have been put forward as a plausible mechanism behind the potential anticancer activity by agents that target oxidative stress in cancer therapy (Okon and Zou, 2015). In the present study, high levels of ROS, as well as low level of antioxidant GSH, was observed in cells treated with Pt-Au NPs. Many anticancer drugs have been known to target deranged cancer biochemical features found in cancer cells by inducing ROS that could be beyond the coping capacity of adapted antioxidant machinery in cancer cells (Coriat et al., 2012). The anticancer drug cisplatin is a well-known example for its extra propensity of inducing oxidative stress in cancer therapy (Ghosh, 2019). Inducing ROS while weakening intracellular GSH are often considered a deadly combination in bringing the demise of cancer cell (Okon and Zou, 2015).

In this study, selective induction of NO in cancer MCF-7 cells by Pt-coated NPs was found as another way to preferentially hit cancer cells. A low level of NO is responsible for the beneficial function achieved by NO as a relaxed vascular tone whereas a high NO can be responsible for the killing of cancer cells (2008). It is clear from the data that NPs caused the production of high NO concentration in the most susceptible MCF-7 cancer cells in comparison to little, if any, in the least susceptible non-cancerous HUVE cells. Sensitivity to NPs-mediated toxicity was strongly dependent on intracellularly induced NO. Recall, NO is a hydrophobic radical molecule that has low reactivity in comparison to other free radicals such as superoxide radicals, and can even terminate lipid peroxidation reactions initiated by strong oxidizing radicals such as hydroxyl radical or nitrogen dioxide radicals (Garrel and Fontecave, 1995). Five-distinct concentration levels of NO in cells have been proposed to explain the opposing effects of this diatomic gaseous molecule (2008). Reactive nitrogen species (RNS) are another group of toxicants that are formed upon reaction with superoxide by NO-producing peroxynitrite with complex consequences in a context-dependent manner (Pacher et al., 2007). NO, therefore, lies at the core of the formation of other RNSs (2008). Similar to the implication of NO in the anticancer potential of NPs in MCF-7 cells

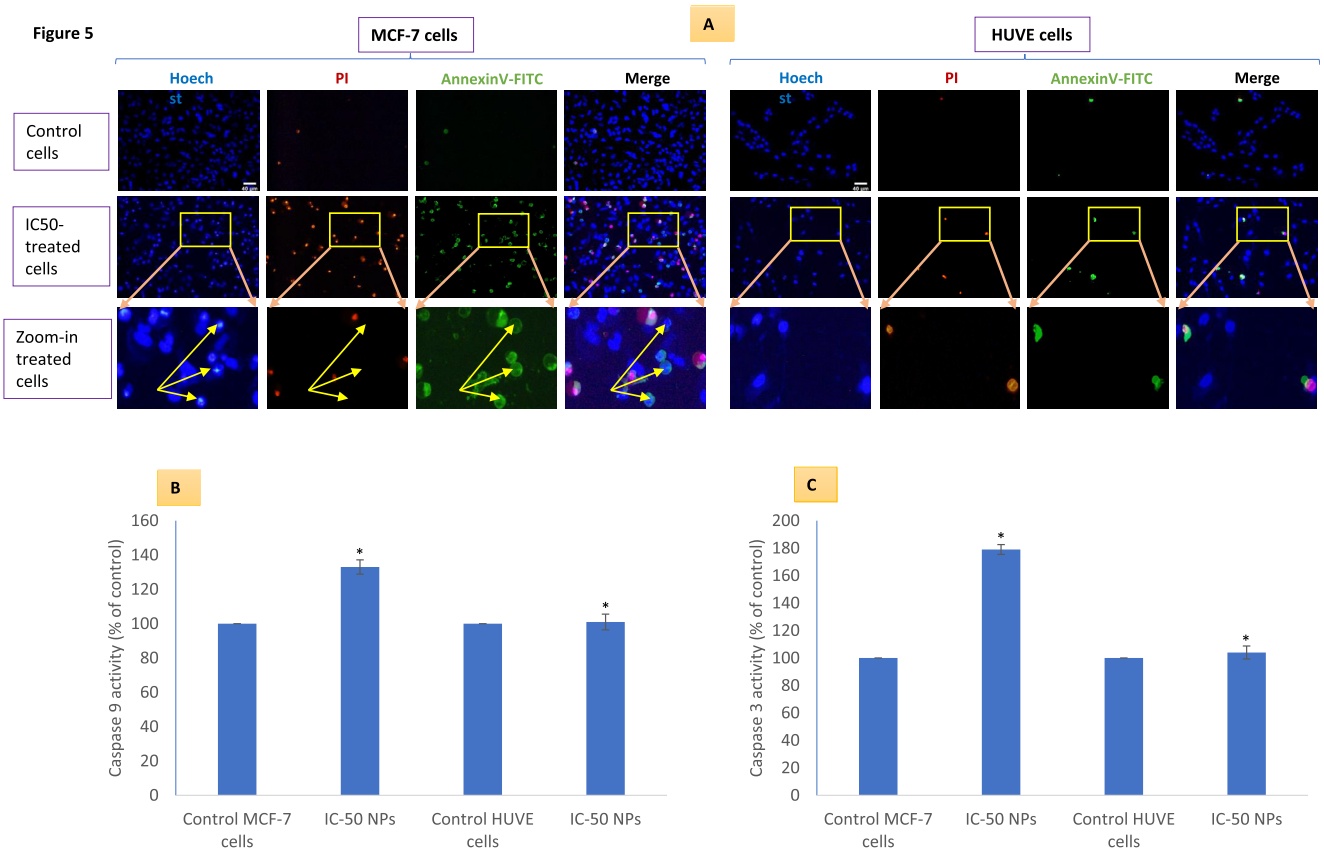

Fig. 5. Potential apoptosis/necrosis was evaluated using the triple-staining technique in MCF-7 and HUVE cells treated at the IC50 of Pt-coated Au NPs (A). Yellow arrows in zoom-in images (see A) of treated MCF-7 cells indicate some cells stained with annexin V but still lack PI staining (early apoptosis). Corresponding (yellow) arrows in Hoechst images point to nuclei that are most intensely stained suggesting a chromatin condensation that is atypical of apoptosis as discussed in the main text. Moreover, differences in nuclear shape perimeter (increased nucleus size and diffused nuclear probe PI/Hoechst fluorescence, a sign of necrosis, in HUVE cells vs compact nucleus size and discrete nuclear probe PI/Hoechst fluorescence, a sign of apoptosis, in MCF-7 cells) also suggested the occurrence different cell death mechanism in MCF-7 and HUVE cells due to NPs treatment. Apoptotic enzyme activity of caspase 9 and 3 are given in (B) and (C) respectively. The scale bar, marked only in control images as a general convention, represents 40 μm captured by a 20 × objective. Data represented are mean ± SD of three identical experiments (n = 3) made in triplicates. *statistically significant difference as compared to the controls ($p < 0.05$).

reported in this study, NO and NO-derived species have been implicated in the anticancer potential of Ag NPs in human osteoblast (hFOB 1.19) cells (Zielinska et al., 2016) and of ZnO NPs in the SH-SY5Y human neuroblastoma (Kim et al., 2015).

Mitochondrial dysfunction has been identified as a central mechanism in anticancer therapy and cytotoxic NPs are well-known inducers of MMP loss in a wide variety of cell lines (Akhtar et al., 2017). Data suggested that Pt-Au NPs elicited significant loss of MMP in both cells but at a much lesser concentration in MCF-7 cells. The underlying mechanism of cell death appeared differently in MCF-7 and HUVE cells when each cell was exposed to their respective IC50 of NPs. MCF-7 cells exhibited annexin V fluorescence that may contain PI fluorescence or might be devoid of PI suggesting a mode of cellular death resembling early and late apoptosis respectively. When closely followed, the nature of chromatin condensation again suggested a cell death occurring via apoptosis. In the present study, caspase 9 and 3 were significantly activated due to NPs in MCF-7 cells while no appreciable change in activity was detected in HUVE cells. On similar grounds examined above, HUVE cells appeared to pass through a necrosis mode of cell death. Gholinejad and co-workers have reported a similar finding for TiO_2 NP-mediated cell death in HUVE cells (Gholinejad et al., 2019). NPs of CdSe/ZnS quantum dots, however, have been reported to induce pyroptosis in hepatic L02 cells that progressed via mitochondrial ROS induction and MMP loss (Akhtar et al., 2017). Again, high concentrations of NO could lead to dysfunction in mitochondria by inhibiting respiration in cells (Thomas, 2001). Inhibition in mitochondrial oxidative phosphorylation can result in adverse outcomes by increased ROS production and decreased conservation of energy. All these adversaries could effectively push MCF-7 cells to the apoptotic mode of cell death. A steeper GSH depletion and overwhelming NO level could have activated an apoptosis-dependent mode of cell death in MCF-7 cancer cells. Higher levels of lipid peroxidation and membrane damage combined with low NO induction could lead to an apoptosis-independent mode of cell death in HUVE cells that were exposed to much higher concentrations of NPs in comparison to MCF-7 cells.

5. Conclusion

Pt-Au NPs appear to selectively kill cancerous MCF-7 over non-cancerous HUVE. We realize two major facts from this study that goes in the favor of anticancer potential of Pt-Au NPs. One reason is the higher quantity of NPs internalization in cancer cells that could lead to cell death in cancerous cells at half of the concentration required for inducing the same degree of toxicity in non-cancerous HUVE cells. The second reason may be the overwhelming level of NO production in cancer cells leading to stress based on excessive nitrosylation and nitration reactions prevalent under excessive NO generation. Moreover, cancer cells are known to possess heterogeneities about redox status, and this is one of the several reasons behind the limited success of ROS-modulating agents in cancer therapy. This study warranted further investigations in other cell lines as well as in vivo models for understanding the mechanism of action at the molecular level.

Declaration of Competing Interest

The authors declare that they have no known competing financial interests or personal relationships that could have appeared to influence the work reported in this paper.

Acknowledgments

The authors extend their appreciation to the Deputyship for Research & Innovation, Ministry of Education in Saudi Arabia for funding this research work through project number IFKSURG-2-653.

References

S. Afifi, N., Abdel-Hamid, E.S., M. Baghdadi, H., 2012. Nuclear Area Factor as a Novel Estimate for Apoptosis in Oral Squamous Cell Carcinoma -Treated Cell Line: A Comparative in-vitro Study with DNA Fragmentation Assay. J. Clin. Exp. Pathol. 02. https://doi.org/10.4172/2161-0681.1000107.

Akhtar, M.J., Ahamed, M., Alhadlaq, H.A., Alshamsan, A., 2017. Mechanism of ROS scavenging and antioxidant signaling by redox metallic and fullerene nanomaterials: Potential implications in ROS associated degenerative disorders. Biochim. Biophys. Acta - Gen. Subj. 1861, 802–813. https://doi.org/10.1016/j.bbagen.2017.01.018.

Akhtar, M.J., Ahamed, M., Alhadlaq, H.A., 2018. Challenges facing nanotoxicology and nanomedicine due to cellular diversity. Clin. Chim. Acta 487, 186–196. https://doi.org/10.1016/j.cca.2018.10.004.

Akhtar, M.J., Ahamed, M., Alhadlaq, H.A., Kumar, S., Alrokayan, S.A., 2020. Mitochondrial dysfunction, autophagy stimulation, and non-apoptotic cell death caused by nitric oxide-inducing Pt-coated Au nanoparticle in human lung carcinoma cells. Biochim. Biophys. Acta - Gen. Subj. 1864,. https://doi.org/10.1016/j.bbagen.2019.129452 129452.

Atale, N., Gupta, S., Yadav, U.C.S., Rani, V., 2014. Cell-death assessment by fluorescent and nonfluorescent cytosolic and nuclear staining techniques. J. Microsc. 255, 7–19. https://doi.org/10.1111/jmi.12133.

Bendale, Y., Bendale, V., Paul, S., 2017. Evaluation of cytotoxic activity of platinum nanoparticles against normal and cancer cells and its anticancer potential through induction of apoptosis. Integr. Med. Res. 6, 141–148. https://doi.org/10.1016/j.imr.2017.01.006.

Bohlen, V., Halbach, O., 2003. Nitric oxide imaging in living neuronal tissues using fluorescent probes. Nitric Oxide - Biol. Chem. 9, 217–228. https://doi.org/10.1016/j.niox.2004.01.001.

Brown, S.D., Nativo, P., Smith, J.A., Stirling, D., Edwards, P.R., Venugopal, B., Flint, D.J., Plumb, J.A., Graham, D., Wheate, N.J., 2010. Gold nanoparticles for the improved anticancer drug delivery of the active component of oxaliplatin. J. Am. Chem. Soc. 132, 4678–4684. https://doi.org/10.1021/ja908117a.

Coriat, R., Nicco, C., Cheŕeau, C., Mir, O., Alexandre, J., Ropert, S., Weill, B., Chaussade, S., Goldwasser, F., Batteux, F., 2012. Sorafenib-induced hepatocellular carcinoma cell death depends on reactive oxygen species production in vitro and in vivo. Mol. Cancer Ther. 11, 2284–2293. https://doi.org/10.1158/1535-7163.MCT-12-0093.

Crowley, L.C., Marfell, B.J., Scott, A.P., Waterhouse, N.J., 2016a. Quantitation of apoptosis and necrosis by annexin V binding, propidium iodide uptake, and flow cytometry. Cold Spring Harb. Protoc. 2016, 953–957. https://doi.org/10.1101/pdb.prot087288.

Crowley, L.C., Marfell, B.J., Waterhouse, N.J., 2016b. Analyzing cell death by nuclear staining with Hoechst 33342. Cold Spring Harb. Protoc. 2016, 778–781. https://doi.org/10.1101/pdb.prot087205.

Darzynkiewicz, Z., Bruno, S., Del Bino, G., Gorczyca, W., Hotz, M.A., Lassota, P., Traganos, F., 1992. Features of apoptotic cells measured by flow cytometry. Cytometry 13, 795–808. https://doi.org/10.1002/cyto.990130802.

Eidet, J.R., Pasovic, L., Maria, R., Jackson, C.J., Utheim, T.P., 2014. Objective assessment of changes in nuclear morphology and cell distribution following induction of apoptosis. Diagn. Pathol. 9. https://doi.org/10.1186/1746-1596-9-92.

Fan, M., Han, Y., Gao, S., Yan, H., Cao, L., Li, Z., Liang, X.J., Zhang, J., 2020. Ultrasmall gold nanoparticles in cancer diagnosis and therapy. Theranostics. https://doi.org/10.7150/thno.42471.

Fink, S.L., Cookson, B.T., 2005. Apoptosis, pyroptosis, and necrosis: Mechanistic description of dead and dying eukaryotic cells. Infect. Immun. 73, 1907–1916. https://doi.org/10.1128/IAI.73.4.1907-1916.2005.

Galadari, S., Rahman, A., Pallichankandy, S., Thayyullathil, F., 2017. Reactive oxygen species and cancer paradox: To promote or to suppress? Free Radic. Biol. Med. https://doi.org/10.1016/j.freeradbiomed.2017.01.004.

Gao, Z., Ye, H., Tang, D., Tao, J., Habibi, S., Minerick, A., Tang, D., Xia, X., 2017. Platinum-Decorated Gold Nanoparticles with Dual Functionalities for Ultrasensitive Colorimetric in Vitro Diagnostics. Nano Lett. 17, 5572–5579. https://doi.org/10.1021/acs.nanolett.7b02385.

Garrel, C., Fontecave, M., 1995. Nitric oxide: Chemistry and biology, in: Analysis of Free Radicals in Biological Systems. Birkhäuser Basel, pp. 21–35. https://doi.org/10.1007/978-3-0348-9074-8_3.

Gholinejad, Z., Khadem Ansari, M.H., Rasmi, Y., 2019. Titanium dioxide nanoparticles induce endothelial cell apoptosis via cell membrane oxidative damage and p38, PI3K/Akt, NF-κB signaling pathways modulation. J. Trace Elem. Med. Biol. 54, 27–35. https://doi.org/10.1016/j.jtemb.2019.03.008.

Ghosh, S., 2019. Cisplatin: The first metal based anticancer drug. Bioorg. Chem. 88. https://doi.org/10.1016/j.bioorg.2019.102925.

Hissin, P.J., Hilf, R., 1976. A fluorometric method for determination of oxidized and reduced glutathione in tissues. Anal. Biochem. 74, 214–226. https://doi.org/10.1016/0003-2697(76)90326-2.

Kim, J.H., Jeong, M.S., Kim, D.Y., Her, S., Wie, M.B., 2015. Zinc oxide nanoparticles induce lipoxygenase-mediated apoptosis and necrosis in human neuroblastoma SH-SY5Y cells. Neurochem. Int. 90, 204–214. https://doi.org/10.1016/j.neuint.2015.09.002.

Kojima, H., Hirotani, M., Nakatsubo, N., Kikuchi, K., Urano, Y., Higuchi, T., Hirata, Y., Nagano, T., 2001. Bioimaging of nitric oxide with fluorescent indicators based on the rhodamine chromophore. Anal. Chem. 73, 1967–1973. https://doi.org/10.1021/ac001136i.

Li, H., Wan, A., 2015. Fluorescent probes for real-time measurement of nitric oxide in living cells. Analyst 140, 7129–7141. https://doi.org/10.1039/c5an01628b.

Mosmann, T., 1983. Rapid colorimetric assay for cellular growth and survival: Application to proliferation and cytotoxicity assays. J. Immunol. Methods 65, 55–63. https://doi.org/10.1016/0022-1759(83)90303-4.

Ohkawa, H., Ohishi, N., Yagi, K., 1979. Assay for lipid peroxides in animal tissues by thiobarbituric acid reaction. Anal. Biochem. 95, 351–358. https://doi.org/10.1016/0003-2697(79)90738-3.

Okon, I.S., Zou, M.H., 2015. Mitochondrial ROS and cancer drug resistance: Implications for therapy. Pharmacol. Res. https://doi.org/10.1016/j.phrs.2015.06.013.

Pacher, P., Beckman, J.S., Liaudet, L., 2007. Nitric oxide and peroxynitrite in health and disease. Physiol. Rev. https://doi.org/10.1152/physrev.00029.2006.

Raudsepp, P., Brüggemann, D.A., Andersen, M.L., 2014. Detection of radicals in single droplets of oil-in-water emulsions with the lipophilic fluorescent probe BODIPY665/676 and confocal laser scanning microscopy. Free Radic. Biol. Med. 70, 233–240. https://doi.org/10.1016/j.freeradbiomed.2014.02.026.

Rawal, P., Siddiqui, H., Hassan, M., Choudhary, M.C., Tripathi, D.M., Nain, V., Trehanpati, N., Kaur, S., 2019. Endothelial cell-derived TGF-β promotes epithelial-mesenchymal transition via CD133 in HBx-infected hepatoma cells. Front. Oncol. 9, 308. https://doi.org/10.3389/fonc.2019.00308.

Sawai, H., Domae, N., 2011. Discrimination between primary necrosis and apoptosis by necrostatin-1 in Annexin V-positive/propidium iodide-negative cells. Biochem. Biophys. Res. Commun. 411, 569–573. https://doi.org/10.1016/j.bbrc.2011.06.186.

Sayes, C.M., Gobin, A.M., Ausman, K.D., Mendez, J., West, J.L., Colvin, V.L., 2005. Nano-C60 cytotoxicity is due to lipid peroxidation. Biomaterials 26, 7587–7595. https://doi.org/10.1016/j.biomaterials.2005.05.027.

Smiley, S.T., Reers, M., Mottola-Hartshorn, C., Lin, M., Chen, A., Smith, T.W., Steele, G. D., Chen, L.B., 1991. Intracellular heterogeneity in mitochondrial membrane potentials revealed by a J-aggregate-forming lipophilic cation JC-1. Proc. Natl. Acad. Sci. 88, 3671–3675. https://doi.org/10.1073/pnas.88.9.3671.

Thomas, D.D., 2001. The biological lifetime of nitric oxide: Implications for the perivascular dynamics of NO and O2. Proc. Natl. Acad. Sci. 98, 355–360. https://doi.org/10.1073/pnas.011379598.

Ullah, S., Ahmad, A., Wang, A., Raza, M., Jan, A.U., Tahir, K., Rahman, A.U., Qipeng, Y., 2017. Bio-fabrication of catalytic platinum nanoparticles and their in vitro efficacy against lungs cancer cells line (A549). J. Photochem. Photobiol. B Biol. 173, 368–375. https://doi.org/10.1016/j.jphotobiol.2017.06.018.

Wang, H., Joseph, J.A., 1999. Quantifying cellular oxidative stress by dichlorofluorescein assay using microplate reader. Free Radic. Biol. Med. 27, 612–616.

Welder, A.A., 1992. A primary culture system of adult rat heart cells for the evaluation of cocaine toxicity. Toxicology 72, 175–187.

Xu, X., An, H., Zhang, D., Tao, H., Dou, Y., Li, X., Huang, J., Zhang, J., 2019. A self-illuminating nanoparticle for inflammation imaging and cancer therapy. Int. J. Agric. Stat. Sci. 14, eaat2953. https://doi.org/10.1126/sciadv.aat2953.

Zielinska, E., Tukaj, C., Radomski, M.W., Inkielewicz-Stepniak, I., 2016. Molecular mechanism of silver nanoparticles-inducedhuman osteoblast cell death: Protective effect of inducible nitric oxide synthase inhibitor. PLoS One 11. https://doi.org/10.1371/journal.pone.0164137.

Further Reading

Thomas, D.D., Ridnour, L.A., Isenberg, J.S., Flores-Santana, W., Switzer, C.H., Donzelli, S., Hussain, P., Vecoli, C., Paolocci, N., Ambs, S., Colton, C.A., Harris, C.C., Roberts, D.D., Wink, D.A., 2008. The chemical biology of nitric oxide: Implications in cellular signaling. Free Radic. Biol. Med. 45, 18–31. https://doi.org/10.1016/j.freeradbiomed.2008.03.020.